Journal of Optometry 000 (2025) 100587



Contents lists available at ScienceDirect

Journal of Optometry

journal homepage: www.journalofoptometry.org



Original Article

Opto-biomechanical simulation of keratoconus development in emmetropic eyes

Hosna Ghaderi^a, Marta Jiménez García^{b,c,d}, Carina Koppen^{a,e}, Jos Rozema^{a,e,*}

- ^a Visual Optics Lab Antwerp (VOLANTIS), Faculty of Medicine and Health Sciences, Antwerp University, Wilrijk, Belgium
- ^b GIMSO, Institute for Health Research Aragón, Hospital Universitario Miguel Servet, Zaragoza, Spain
- ^c UFR, Department of Ophthalmology, University Hospital Miguel Servet, Zaragoza, Spain
- ^d ARCCA, Department of Ophthalmology, Hospital Nuestra Señora de Gracia, Zaragoza, Spain
- e Dept. of Ophthalmology, Antwerp University Hospital, Edegem, Belgium

ARTICLE INFO

Key words: Keratoconus Cornea Finite element modelling

ABSTRACT

Purpose: To assess how different corneas respond to a standardized structural weak spot in different sizes and locations using the finite element method depending on their initial geometry.

Method: The corneal meshes of 5 randomly selected emmetropic SyntEyes with different biometry and optical properties were generated using MATLAB and ANSYS. To simulate keratoconus development, a local stiffness reduction of up to 60 % of the original value was implemented in three locations (central, 1 mm, and 2 mm inferior) with a diameter of 2 mm for each cornea. From this, tangential corneal power maps were calculated.

Results: Local weakening causes the formation of a conical deformation at the site of the weak spot and, for an inferior weak spot, a superior flattening. At the center of the weak spot, the cornea becomes thinner by $50~\mu m$, while the maximum anterior curvature increased by an average of $51.76 \pm 1.38D$ and the posterior curvature by an average of $-7.45 \pm 0.15D$ for the central keratoconus. The anterior surface area increases by $0.88 \pm 0.29~mm^2$ and $0.85 \pm 0.03~mm^2$ for a central and inferior keratoconus, respectively. The corresponding values for the posterior surface were $1.10 \pm 0.03~mm^2$ and $1.06 \pm 0.03~mm^2$.

Conclusion: The shape of a keratoconic cornea is not only determined by the response to a local structural weakening, but also by its original corneal shape. This understanding may help enhance early detection and monitoring techniques for keratoconus progression.

Introduction

The biomechanical stability of the cornea is maintained through a highly organized arrangement of collagen fibers within the stroma that provides both strength and elasticity. 1,2 In keratoconus, this collagen matrix is disrupted, leading to a localized biomechanical instability.³ This causes the cornea to gradually become thinner and assume a conical shape, that manifests optically as large amounts of higher order aberrations and a reduced visual image quality. Keratoconic eyes typically cannot be fully corrected by standard spectacles, except for the earliest cases. Instead, the most common approach is to use rigid gas permeable (RGP) contact lenses that provide a more regular first surface for light to pass through and reduce the influence of the anterior corneal surface through index matching. However, RGP users can experience discomfort in the long term. In those cases, scleral lenses should be proposed as a possible alternative previous to corneal transplant. 5 Meanwhile, the primary therapeutic intervention for keratoconus is corneal cross-linking (CXL), a procedure designed to strengthen the corneal tissue to stop the

progression of the disease. This involves applying riboflavin (vitamin B2) to the cornea and then exposing it to ultraviolet A (UVA) light to increase the collagen cross-links within the cornea, making it stiffer and more resistant to deformation. While effective in slowing or stopping the progression of keratoconus, CXL does not reverse the damage already done. In more advanced cases, when the best-corrected visual image quality becomes inadequate for the patient, or the cornea becomes dangerously thin, a corneal transplantation may be considered. However, this procedure is costly and carries a risk of graft rejection, infections, and other complications. It is therefore essential to ensure that the cornea does not reach these advanced stages by crosslinking keratoconus cases confirmed as progressive in the earliest possible stage. For this reason, imaging techniques such as corneal topography and optical coherence tomography are essential to screen those in need of treatment. S-10

The exact cause of the structural weakening in keratoconus is not completely understood, but it is believed to involve hereditary predisposition, 11,12 systemic influences, and behavioral factors such as

E-mail address: jos.rozema@uantwerpen.be (J. Rozema).

https://doi.org/10.1016/j.optom.2025.100587

Received 10 August 2024; Accepted 25 September 2025

1888-4296/© 2025 The Author(s). Published by Elsevier España, S.L.U. on behalf of Spanish General Council of Optometry. This is an open access article under the CC BY-NC-ND license (http://creativecommons.org/licenses/by-nc-nd/4.0/)

Please cite this article as: H. Ghaderi et al., Opto-biomechanical simulation of keratoconus development in emmetropic eyes, Journal of Optometry (2025), https://doi.org/10.1016/j.optom.2025.100587

^{*}Corresponding author.

H. Ghaderi et al. Journal of Optometry 00 (2025) 100587

frequent eye rubbing. 13-15 To further investigate the importance of the corneal biomechanical properties, researchers have employed various modeling techniques to understand the underlying issues that lead to the development and progression of keratoconus. Carvalho et al., ¹⁶ for example, developed a Finite Element Model (FEM) of the cornea to predict keratoconus-like behavior based on its local biomechanical material properties under varying conditions such as elasticity changes and intraocular pressure. Their model demonstrated that local changes in material properties induce the characteristic conical deformation seen in keratoconus. Similarly, Roy and Dupps¹⁷ created patient-specific computational models to study keratoconus progression and the effect of crosslinking treatments by incorporating clinical tomography and intraocular pressure measurements to simulate changes in corneal curvature and higher-order aberrations. They also found that regional reductions in corneal hyperelastic properties replicated keratoconic topographic features, providing a useful tool for evaluating treatment responses and disease progression. Further numerical simulations by Falgayrettes et al. 13 found that softening of specific corneal layers, particularly the posterior stroma, could lead to the conical deformation and thinning characteristic of keratoconus. Their models also highlighted the impact of eye rubbing on the biomechanical stress distribution within the cornea, which could exacerbate the progression of the disease as eye rubbing creates shear stress on the corneal tissue, causing mechanical damage to the delicate interlamellar cross-links that provide structural integrity to the cornea. Indirectly, the mechanical stress from eye rubbing can also induce keratocyte apoptosis, a process where cells undergo a programmed death. 3,18,19 This cellular damage can lead to an increase in the production of matrix catabolic proteins, which break down the extracellular matrix components. Additionally, the production of essential structural components such as collagen and ground substances can be impaired.²⁰

Additional studies introduced advanced numerical models to capture the complexity of corneal biomechanics. Pandolfi et al. 19 proposed a microstructural model that considers the interaction between collagen fibrils and cross-links within the stromal matrix. Their results showed that the weakening of cross-links could lead to a marked increase in the deformability of the cornea, potentially triggering the progression of keratoconus. Köry et al.²¹ developed a discrete-to-continuum mathematical model for corneal biomechanics, illustrating how localized reductions in collagen stiffness led to macroscopic thinning and increased curvature of the anterior and posterior corneal surfaces, consistent with keratoconus progression. Meanwhile, Fantaci et al.²² proposed a continuum-based keratoconus growth model that accounts for the structural changes in the underlying tissue during disease progression to provide insights into how extracellular matrix degradation, tissue remodeling, and collagen fiber disorganization contribute to the pathology. Their findings suggest that keratoconus progression may be driven by a combination of biomechanical weakening and growth mechanisms, emphasizing the importance of early detection and intervention

While previous studies confirmed that the presence of weak areas can progressively deform the cornea, the influence of the initial corneal shape on the keratoconic shape changes has not been investigated. Hence this study uses the finite element method to study whether the same structural weakness induced on different healthy corneas would produce the same keratoconus pattern.

Method

This analysis starts from 5 randomly selected emmetropic corneas produced by the SyntEyes model, a higher-order statistical eye model designed to generate synthetic biometric data sets with statistical properties identical to those of the original data set of healthy Belgian adults.²³ The properties are provided in Table 1.²³ The following section describes the methodology, including the generation of synthetic corneal geometries, the material properties used, and the finite element analysis approach applied.

Table 1 Geometrical parameters (*mm*).

	r_{ca}	r_{cp}	CCT	S
Case 1	8.02	6.53	0.57	0.08 D
Case 2	7.57	6.24	0.52	-0.43 D
Case 3	7.90	6.68	0.55	0.36 D
Case 4	7.77	6.45	0.58	0.30 D
Case 5	8.04	6.52	0.53	-0.39 D
Mean \pm SD	7.86 ± 0.15	6.48 ± 0.12	$\textbf{0.55} \pm \textbf{0.02}$	0.01 ± 0.29

 r_{ca} , r_{cp} ; anterior and posterior corneal radius of curvature; CCT: central corneal thickness; S: spherical refractive error.

Geometry and mesh

The first step of the modelling involves defining the corneal geometry and generating an appropriate computational mesh. The elevations of each corneal surface were initially described as two sets of Zernike coefficients (45 coefficients over a 6.5 mm diameter area, each) that were converted into point clouds in a Cartesian coordinate system using Matlab (R2023a, The MathWorks, Natick, MA, USA). These point clouds were extrapolated to a limbal diameter of 12 mm, close to the average diameter of an adult cornea, ²⁴ by fitting a quadratic surface to both the anterior and posterior cornea surfaces:

$$z(x,y) = c_1 + c_2 x + c_3 y + c_4 x^2 + c_5 x y + c_6 y^2$$
 (1)

where z represents the corneal elevation, x and y are the cartesian coordinates on the corneal surface, and coefficients c_1 to c_6 are fitted to the point cloud of each corneal surface. The center of this fitted surface was subsequently replaced by the original surface over the initial 6.5 mm diameter. But as this leads to discontinuities at the interface between the original and fitted surfaces, a smoothing algorithm was applied to prevent convergence issues during finite element analysis and ensure a smooth optical surface for accurate calculations (Fig. 1). Next, to create the corneal volume, the posterior surface was shifted backwards by the value of the central corneal thickness (CCT), thus completing the point cloud model. This model was then converted into STL (stereolithography) files through triangulation, and into INP mesh files using MATLAB PDE (Partial Differential Equation) functions. Finally, these INP meshes were imported into Ansys Mechanical (2023 R2, Ansys Inc, Southpointe, PA, USA) for tetrahedral remeshing using the SOLID185 element and the finite element analysis itself (Fig. 2).

Material properties

With the corneal geometry and mesh defined, the next critical step is to assign appropriate material properties that accurately represent the mechanical behavior of the corneal tissue (Table 2). In this study, the anisotropic, nonlinear mechanical response of the cornea is modeled using the Holzapfel-Gasser-Ogden (HGO) hyperelastic material model, implemented through the PolyUMod material library in ANSYS Mechanical. The HGO model is specifically developed to describe the behavior of fiber-reinforced soft biological tissues, such as the cornea, where collagen fibers are embedded within a hyperelastic ground matrix. This formulation captures both the isotropic response of the matrix and the directional stiffness introduced by the collagen fibers.

The strain energy density function in the HGO model is decomposed into two parts: a deviatoric (volume-preserving) part and a volumetric (compressibility) part. Mathematically, the total strain energy potential is expressed as:

$$W = W_{dev} + W_{vol} \tag{2}$$

Journal of Optometry 00 (2025) 100587

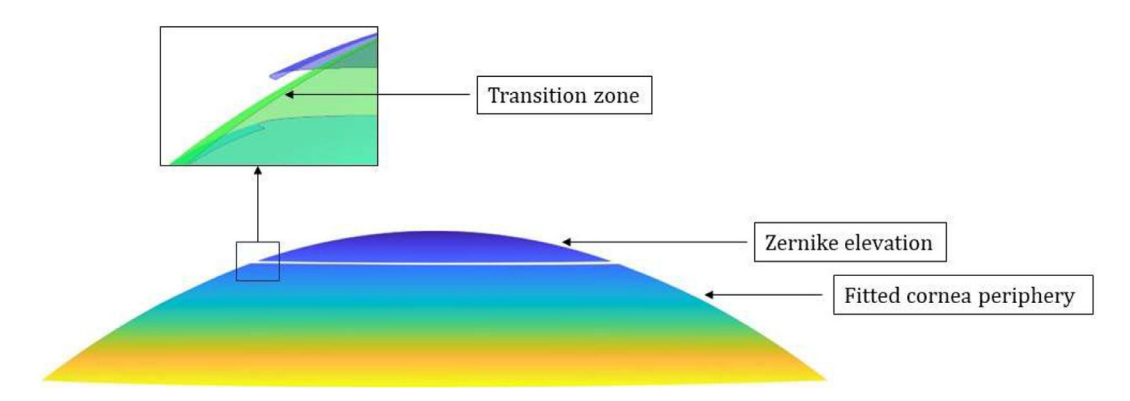


Fig. 1. Visualization of corneal geometry. Zernike elevation corresponds to the original elevation data, which is fitted with the quadratic surface; Fitted corneal periphery: the peripheral cornea area is extrapolated using the quadratic function. Inset: Transition between the central and peripheral areas of the cornea using a smoothing algorithm.



Fig. 2. The final mesh.

Table 2Material properties.

H. Ghaderi et al.

	C_{10}	k_1	k_2	k
Cornea	0.03 (MPa)	0.02 (MPa)	400	5.56 (MPa)

The deviatoric component is formulated based on a Neo-Hookean matrix model and an exponential fibre reinforcement term, as follows:

$$W_{dev} = \frac{C_{10}}{2} (\bar{I}_1 - 3) + \frac{k_1}{2k_2} \sum_{i=4,6} \left[\exp(k_2 E_i^2) - 1 \right]$$
 (3)

where C_{10} is the Neo-Hookean stiffness parameter, while k_1 and k_2 are material parameters that define the stiffness and nonlinearity of the fibre reinforcement, respectively.

 \overline{I}_1 is the first invariant of the isochoric left or right Cauchy-Green deformation tensor:

$$\overline{I}_1 = tr(\overline{b}) \tag{4}$$

Here, \overline{b} is the deviatoric part of the left Cauchy-Green deformation tensor b, F denotes the deformation gradient tensor and $J=\det(F)$ represents the local volume ratio:

$$\overline{\boldsymbol{b}} = J^{-2\beta} \boldsymbol{b} \tag{5}$$

$$b = FF^{T} \tag{6}$$

The volumetric part accounts for the material's resistance to volume change:

$$W_{vol} = \frac{k}{2}(J-1)^2 \tag{7}$$

with k the bulk modulus, reflecting the material's resistance to volume change. The anisotropic contribution of the fibre families is introduced via the strain measure E_i defined for each fibre direction as:

$$E_i = d(I_{4i}^* - 3) + (1 - 3d) \langle I_{4i}^* - 1 \rangle$$

Here, d is the dispersion parameter, where if d=0, the fibres are perfectly aligned, and if d=0.333, the fibers are oriented randomly. The latter value was used in this study. I_{4i}^* is modified fourth invariant represents the square of fibre stretch in the direction a_i :

$$I_{4i}^* = (\boldsymbol{F}.\boldsymbol{a}_i).(\boldsymbol{F}.\boldsymbol{a}_i)$$

In this study, two perpendicular fibre families were modelled to represent the preferred collagen orientations in the corneal stroma.

Stress-free configuration

Creating accurate mechanical models of the eye is challenging as the intraocular pressure (IOP) induces a tension that reshapes its tissues. Clinical measurements (or SyntEyes) typically reflect this pressurized state, so using these measurements directly in a finite element method (FEM) model would result in exaggerated geometric changes. Conversely, excluding IOP from the model fails to simulate the stress it would cause, making it an inaccurate representation of *in vivo* conditions. To address this, the eye's stress-free configuration (the hypothetical condition without IOP) must be estimated by iteratively solving an inverse nonlinear static problem. This process used an initial nodal pressure of 16 mmHg uniformly applied to the posterior corneal surface and assumed that the boundary conditions were that the corneal edge was fixed and attached to the sclera, maintained by the ocular tissues.

Corneal weak spot

After achieving stress-free configuration, we simulated the development of keratoconus by introducing a weak spot on the cornea. This weak spot was designed as a linear stiffness reduction by up to 60 % of the original value using APDL (Ansys Parametric Design Language) over a circular area with a 2-mm diameter, at three locations (central, 1 mm, and 2 mm inferiorly). The weak spot was surrounded by a 1.5 mm wide transition zone (Fig. 3a-c). The stiffness transition was defined to maintain a constant stiffness reduction within the focal weak spot, with a

Journal of Optometry 00 (2025) 100587

H. Ghaderi et al.

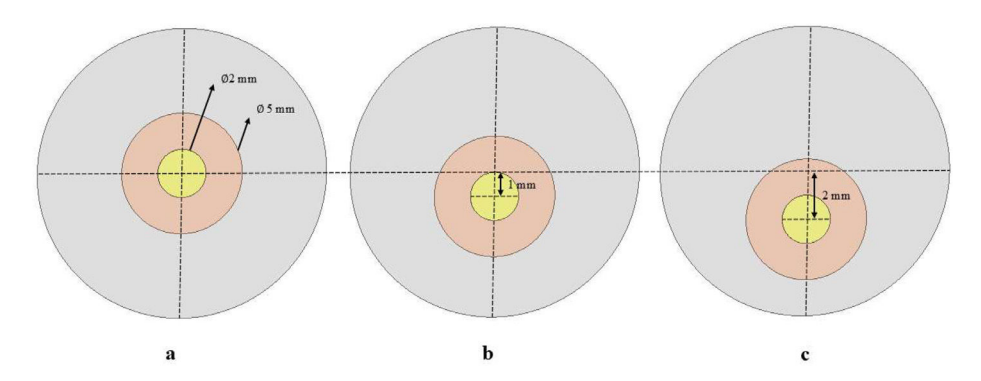


Fig. 3. Size and location of the corneal weak spots considered: a) Central with 2 mm diameter, b) 1mm Inferior, c) 2 mm Inferior. Gray indicates the area with a normal stiffness value, red the transition zone, and yellow the keratoconus zone.

linearly increasing stiffness gradient in the surrounding transition zone towards the boundary of the weak area with the healthy cornea.

Data analysis

After determining the corneal deformation due to the weak spot, the central 6.5 mm of the anterior and posterior surface is exported as point clouds. These point clouds were then fitted by an 8th order Zernike polynomial expansion in MATLAB, after which the tangential curvature was calculated. These curvatures were subsequently compared between cases, size, and location of weak spots, and reduction methods.

Results

Mesh convergence

A convergence analysis was conducted in order to determine the optimal mesh density for the finite element modelling. This was performed at four density levels for all five corneas without weak spot, using the apical displacement and maximum curvature changes under normal intraocular pressure (16 mmHg) as a reference (Table 3). Although mesh level 3 was deemed sufficient for structural simulations, mesh level 4 was employed across all models to guarantee both structural accuracy and a sufficiently smooth surface for the curvature maps.

Tangential curvature

The following gives an overview of the curvature changes due to the corneal weak spot, listed by the location (Fig. 4, Table 4). Maps of the power changes are provided in Supplement A.

A central weakness with a uniform center produces a pronounced central bulging, typical of a severe keratoconus. The curvature maps depict a steep cone formation at the weak spot, with a sharp transition from the affected area to the healthy tissue. The maximum anterior curvature change for central weakness was between 6.70D and 9.74D

The most inferior weak spots show an inferior steepening reminiscent of a pellucid marginal degeneration with a crab claw pattern. The change in maximum anterior curvature for 1 mm inferior

weakness was between 11.91D and 23.23D 40.41D, and -1.62D and 3.89D for the posterior cornea. Here, the topographical changes are almost the same for all eyes, probably due to the more extreme deformations (Supplement A).

Pachymetry

The corneal thickness reduced at the center of the weak spots that varied by $50 \, \mu m$, depending on the case, and location. The strongest reduction was seen for the central keratoconus scenario (about $60 \, \mu m$ reduction).

In contrast, the thickness reduction for inferior keratoconus was less pronounced, with only a $10-20~\mu m$ decrease in thickness at the center of the weak spots.

Surface area

The anterior surface area increases by $0.88 \pm 0.29 \ mm^2$ and $0.85 \pm 0.03 \ mm^2$ for a central and inferior keratoconus, respectively. The corresponding values for the posterior surface were $1.10 \pm 0.03 \ mm^2$ and $1.06 \pm 0.03 \ mm^2$.

Discussion

This study employed finite element analysis to evaluate the impact of initial corneal geometry on corneal shape changes during the onset of keratoconus. To this end, a mechanical model was used to generate a weak spot at various locations on emmetropic corneas. The observations provide detailed curvature and pachymetry data that showed different deformation patterns, reflecting how keratoconus might develop in response to the same structural weakness applied to normal corneas. The resulting topography maps clearly show how local weakening of the cornea leads to the formation of a cone nearby that location. Furthermore, for inferior weaknesses this goes accompanied by a flattening in the adjacent areas, as previously described. ²⁵

In the simulations, the localized reduction in corneal stiffness leads to a distinct, pronounced central bulging indicative of a keratoconus (Fig. 4) that becomes more pronounced with as the local stiffness reduces (Fig. 5). Furthermore, the inferior keratoconus simulations highlight a well-known characteristic of this pathology, with >90~% of the keratoconus showing a

Table 3Mesh densities considered over five corneas.

	Nodes (Mean ± SD)	Elements (Mean ± SD)	Apical displacement (μm)	Curvature changes (%)
Level 1	35,724.20 ± 811.73	20,015.20 ± 503.20	79.54 ± 2.99	0
Level 2	82,003.40 ± 1446.46	46,543.40 ± 844.15	79.74 ± 3.02	0.04
Level 3	341,043.20 ± 7375.85	196,374.00 ± 4331.39	80.44 ± 2.94	0.06
Level 4	542,899.20 ± 10,310.32	$314,536.20 \pm 5981.16$	80.50 ± 2.96	0.03

H. Ghaderi et al.

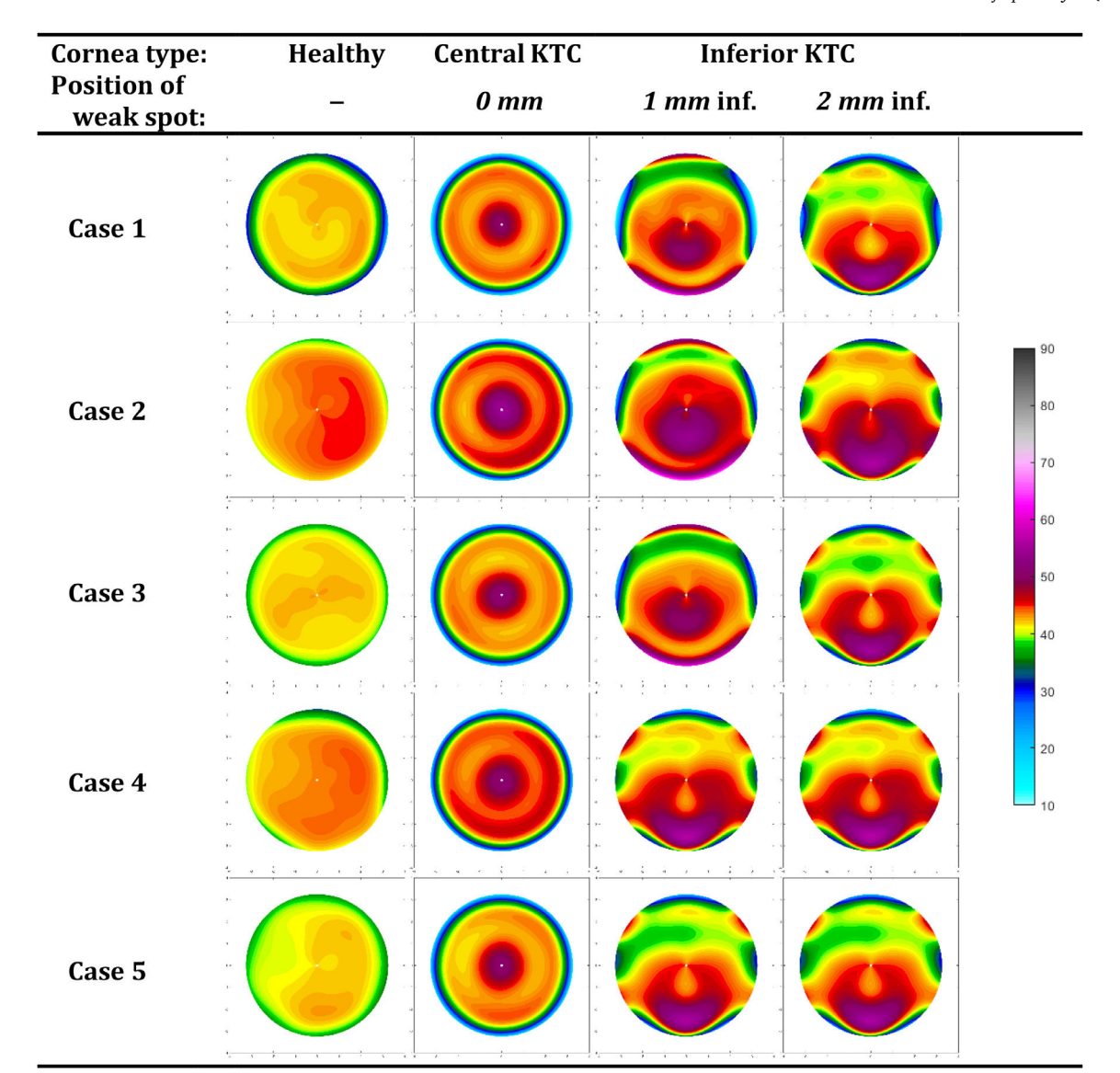


Fig. 4. Anterior tangential curvature maps (in dioptre) for all cases (KTC: keratoconus).

corneal thinnest point decentered both inferiorly and temporally. ²⁶ The curvature maps clearly demonstrate the steepening effect in the inferior part of the cornea, with adjacent areas presenting some flattening as a coupling effect. This uneven deformation pattern aligns with clinical observations of inferior keratoconus, where the cone typically forms below the central cornea, resulting in irregular astigmatism and distorted vision. As shown in Fig. 4, weak spots at the most inferior position form a pattern consistent with pellucid marginal degeneration. This confirms that, at least topographically, pellucid marginal degeneration may indeed represent an inferior form of keratoconus. However, it is often considered a separate condition due to its distinct physiological characteristics, possibly influenced by its proximity to the limbus. Despite the clear differences observed between the topographical patterns of the individual eyes (columns in Figs. 4), the changes in topographical patterns look remarkably similar between eyes (Supplement A).

While this study may not have immediate clinical applications, it provides valuable insights into the role of initial corneal shape variations in determining the progression of keratoconus. Our findings demonstrate that the same degree of weakening can lead to significant progression in some cases, as indicated by $K_{\rm max}$, while in others, the progression

remains minimal, solely due to differences in the initial corneal curvature. Such analyses can only be performed through modeling, as the pre-keratoconic shape of the cornea is rarely available in clinical settings since most patients seek ophthalmologic evaluation only after symptoms appear.

These findings contribute to understanding how different phenotypes of keratoconus develop and suggest that some healthy corneal geometries may lead to larger amounts of deformation should they ever develop keratoconus. This knowledge can aid clinicians in differentiating between patients who may require more intensive follow-up and those with a more stable condition. Ultimately, the research supports a move towards a more personalized approach to keratoconus management. Furthermore, our results may help refine the area of interest for customized topography-guided corneal collagen cross-linking, as current treatments still irradiate the central 8 mm by default. The study by Cassagne et al. 27 suggests that a more individualized approach could be beneficial in determining the most effective treatment zone. By better defining the area of interest for intervention, we may improve the long-term outcomes of keratoconus management.

Table 4

Maximum anterior and posterior corneal power and pachymetry for all cases, and all weak spot positions. Value between brackets is the change from baseline.

Cornea type:		Healthy	Central KTC	Inferior KTC	
Position of weak spot:		-	0 mm	1 mm inf.	2 mm inf.
Case1	Anterior	43.12	50.44(+7.32)	65.49(+22.37)	55.07(+11.95)
	Posterior	-5.67	-7.37(+1.70)	-7.36(+1.69)	-9.06(+3.39)
	Pachymetry	0.57	0.51(-0.06)	0.52(-0.05)	0.56(-0.01)
Case 2	Anterior	45.11	54.85(+9.74)	68.34(+23.23)	55.94(+10.83)
	Posterior	-5.98	-7.79(+1.81)	-7.60(+1.62)	-9.86(+3.88)
	Pachymetry	0.52	0.47(-0.05)	0.47(-0.5)	0.51(-0.01)
Case 3	Anterior	42.90	51.42(+8.52)	62.97(+20.07)	55.03(+12.13)
	Posterior	-5.82	-7.31(+1.49)	-7.30(+1.48)	-9.34(+3.52)
	Pachymetry	0.55	0.50(-0.05)	0.50(-0.05)	0.54(-0.01)
Case 4	Anterior	44.46	51.16(+6.70)	56.37(+11.91)	56.59(+12.13)
	Posterior	-5.78	-7.37(+1.59)	-9.67(+3.89)	-9.57(+3.79)
	Pachymetry	0.58	0.53(-0.05)	0.57(-0.01)	0.57(-0.01)
Case 5	Anterior	42.89	50.94(+8.05)	55.86(+12.97)	55.88(+12.99)
	Posterior	-5.64	-7.42(+1.78)	-9.42(+3.78)	-9.40(+3.76)
	Pachymetry	0.53	0.48(-0.05)	0.52(-0.01)	0.52(-0.01)
Average	Anterior	43.69 ± 0.83	51.76 ± 1.38	61.80 ± 4.33	55.70 ± 0.51
	Posterior	-5.77 ± 0.10	-7.45 ± 0.15	-8.27 ± 0.91	-9.44 ± 0.23
	Pachymetry	0.55 ± 0.02	0.49 ± 0.01	0.51 ± 0.02	0.54 ± 0.02

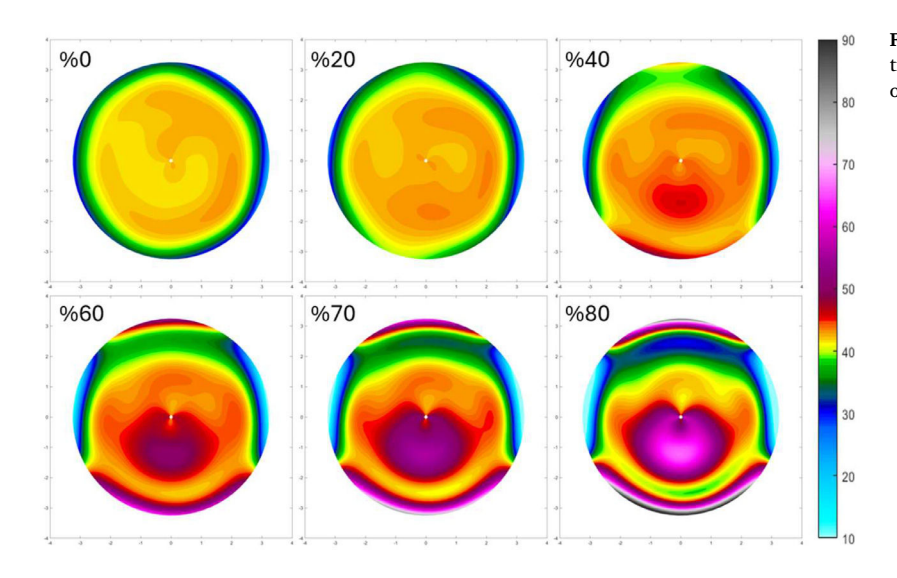


Fig. 5. Anterior curvature changes during keratoconus evolution for Case 1 with a 2-mm weakness located of 1 mm inferiorly, for local stiffness reductions from 0 % to 80 %.

Conclusion

Although the mechanical response to a corneal weak spot is fairly similar between eyes, the resulting topographical maps can be rather different due to the influence of the original corneal shape. These structural alterations underscore the importance of considering corneal geometry in the diagnosis, monitoring, and treatment of keratoconus. Understanding the role of corneal shape can lead to more precise and effective therapeutic strategies, potentially improving patient outcomes and slowing the progression of keratoconus.

Conflicts of interest

The authors have no conflicts of interest to declare.

Acknowledgements

This project has received funding from the European Union's Horizon 2020 research and innovation program under the Marie Skłodowska-Curie grant agreement No 956720.

Supplementary materials

Supplementary material associated with this article can be found in the online version at doi:10.1016/j.optom.2025.100587.

References

- Meek KM, et al. Changes in collagen orientation and distribution in keratoconus corneas. Invest Ophthalmol Vis Sci. 2005;46:1948–1956.
- Meek KM, Knupp C. Corneal structure and transparency. Prog Retin Eye Res. 2015;49:1–16.
- Roy AS, Shetty R, Kummelil MK. Keratoconus: a biomechanical perspective on loss of corneal stiffness. *Indian J Ophthalmol.* 2013;61:392–393.
- Zhang XH, Li X. Effect of rigid gas permeable contact lens on keratoconus progression: a review. Int J Ophthalmol. 2020;13:1124–1131.
- Koppen C, et al. Scleral Lenses Reduce the Need for Corneal Transplants in Severe Keratoconus. Am J Ophthalmol. 2018;185:43–47.
- Wollensak G, Spoerl E, Seiler T. Riboflavin/ultraviolet-A-induced collagen crosslinking for the treatment of keratoconus. Am J Ophthalmol. 2003;135:620–627.
- Vinciguerra R, et al. Corneal Cross-linking for Progressive Keratoconus: up to 13 Years of Follow-up. J Refract Surg. 2020:838–843.
- Ruiseñor Vázquez PR, et al. Pentacam scheimpflug tomography findings in topographically normal patients and subclinical keratoconus cases. Am J Ophthalmol. 2014;158.

JID: OPTOM [m5GeS;November 4, 2025;17:00]

H. Ghaderi et al.

Journal of Optometry 00 (2025) 100587

- 9. Ambrósio R, et al. Optimized Artificial Intelligence for Enhanced Ectasia Detection Using Scheimpflug-Based Corneal Tomography and Biomechanical Data. Am J Ophthalmol. 2023;251:126-142.
- 10. Saad A. Validation of a New Scoring System for the Detection of Early Forme of Keratoconus. Int J Keratoconus Ectatic Corneal Dis. 2012:1:100-108.
- 11. Wang Y, Rabinowitz YS, Rotter JI, Yang H. Genetic epidemiological study of keratoconus: evidence for major gene determination. Am J Med Genet. 2000;93:403-409.
- 12. Rabinowitz YS, Galvis V, Tello A, Rueda D, García JD. Genetics vs chronic corneal mechanical trauma in the etiology of keratoconus. Exp Eye Res. 2021;202:108328.
- 13. Falgayrettes N, Patoor E, Cleymand F, Zevering Y, Perone JM. Biomechanics of keratoconus: two numerical studies. PLoS One. 2023;18:1–25.
- 14. McMonnies CW. Mechanisms of rubbing-related corneal trauma in keratoconus. Cornea, 2009;28:607-615.
- 15. Moran S, Gomez L, Zuber K, Gatinel D. A Case-Control Study of Keratoconus Risk Factors. Cornea. 2020;39(6):697-701.
- Carvalho LA, et al. Keratoconus prediction using a finite element model of the cornea with local biomechanical properties. Arq Bras Oftalmol. 2009;72:139–145.
- 17. Roy AS, Dupps WJ. Patient-specific computational modeling of keratoconus progression and differential responses to collagen cross-linking. Invest Ophthalmol Vis Sci. 2011;52:9174-9187
- 18. Zhou D, et al. Fibril density reduction in keratoconic corneas. J R Soc Interface. 2021;18.

- 19. Pandolfi A, Gizzi A, Vasta M. A microstructural model of cross-link interaction between collagen fibrils in the human cornea. Philosophic Transac Royal Soc A.
- 20. Blackburn BJ, Jenkins MW, Rollins AM, Dupps WJ. A review of structural and biomechanical changes in the cornea in aging, disease, and photochemical crosslinking. Front Bioeng Biotechnol, 2019:7.
- 21. Köry J, Stewart PS, Hill NA, Luo XY, Pandolfi A. A discrete-to-continuum model for the human cornea with application to keratoconus. R Soc Open Sci. 2024.
- 22. Fantaci B, Calvo B, Rodríguez JF. Modeling biological growth of human keratoconus: on the effect of tissue degradation, location and size. Comput Biol Med. 2024;180.
- 23. Rozema JJ, Rodriguez P, Navarro R, Tassignon MJ. Synteyes: a higher-order statistical eye model for healthy eyes. Invest Ophthalmol Vis Sci. 2016;57:683-691.
- Consejo A, Llorens-Quintana C, Radhakrishnan H, Iskander DR. Mean shape of the
- human limbus. *J Cataract Refract Surg*, 2017;43:667–672.
 Gatinel D. Challenging the "No Rub, No Cone" Keratoconus Conjecture. *Int J Keratoco* nus Ectatic Corneal Dis. 2018:7:66-81.
- 26. iménez-García M, Ní Dhubhghaill S, Koppen C, Varssano D, R J, T RSG. Baseline Findings in the Retrospective Digital Computer Analysis of Keratoconus Evolution (REDCAKE) Project. Cornea. 2021;40(2):156–167. https://doi.org/10.1186/s40662-016-0038-6. 1.
- Cassagne M, et al. Customized topography-guided corneal collagen cross-linking for keratoconus. J Refract Surg. 2017;33:290-297.